High-Gain and High-Efficiency EER/Polar Transmitters Using Injection-Locked Oscillators

Chi-Tsan Chen, *Member, IEEE*, Tzyy-Sheng Horng, *Senior Member, IEEE*, Kang-Chun Peng, *Member, IEEE*, and Chien-Jung Li, *Member, IEEE*

***Abstract*—The envelope elimination and restoration (EER) approach developed by Kahn and its modern derivative, a polar transmitter, are well recognized as highly efficient amplification schemes. This paper presents an EER/polar dual-mode transmitter using injection-locked oscillators (ILOs). For an EER operation, an ILO that is combined with a mixer and a low-pass filter in the proposed architecture extracts an envelope signal and a phase-modulated RF signal from an input RF signal with complex modulation. The phase-modulated RF signal is then amplified efficiently by a class-E power amplifier (PA). Additionally, the envelope signal is reconstructed at the PA output by modulating the supply voltage of the PA. For a polar operation, the necessary phase modulation and envelope modulation are generated in the digital domain instead. Moreover, the phase-modulated RF signal is injected into an ILO and the ILO output is amplified by a class-E PA while supply-modulated with the envelope signal. For wideband code-division multiple access (WCDMA) signals, the implemented prototype transmitter achieves a 20.8-dB gain and 44% power-added efficiency (PAE) at an average output power of 25.8 dBm. For enhanced data rates for GSM evolution signals, it delivers 26.6 dB of gain and 48.7% PAE at an average output power of 26.6 dBm. Furthermore, to compensate for the AM–AM and AM–PM distortions of the PA, the linearity is improved using static digital predistortion. Experimental results demonstrate that the proposed EER/polar transmitter using ILOs has a high gain, high efficiency, and good linearity.**

***Index Terms*—Enhanced data rates for GSM evolution (EDGE), envelope elimination and restoration (EER), polar transmitter, power amplifier (PA), predistortion, wideband code-division multiple access (WCDMA).**

I. Introduction

CHARACTERIZED by their high efficiency and high linearity, power amplifiers (PAs) are more critical than ever in modern wireless communication systems, which use nonconstant envelope modulation schemes with a high peak-to-average power ratio (PAPR) [1]. To meet strict linearity requirements, conventional linear PAs (e.g., class-A and class-AB designs) often operate in the power back-off region, subsequently reducing the average efficiency. Therefore, linear amplification methods using highly efficient switch-mode or saturated PAs have been thoroughly investigated, including envelope elimination and restoration (EER) [2]–[5], linear amplification with nonlinear components (LINC) [6], polar modulation [7]–[9], hybrid EER [10], [11], and envelope tracking (ET) [12]–[15]. Among the several efficiency-enhancement schemes, EER developed by Kahn in 1952 is highly promising due to its very high efficiency with good linearity [2]. A Kahn EER transmitter operates under the principle of splitting an input RF signal with a complex modulation into an envelope signal and a phase-modulated RF signal. In a traditional approach, the former and the latter signals can be generated by sending the input-modulated RF signal into an envelope detector and a limiter, respectively. The phase-modulated RF signal is then amplified efficiently by a switch-mode PA, while preserving the phase modulation (PM) at the PA output. Additionally, the amplitude modulation (AM) is restored by modulating the supply voltage of the PA with the envelope signal. In practice, implementing an envelope detector and a limiter is a quite challenging task for a modulation signal with a high PAPR [4], [16]. Moreover, other system-related design issues include the efficiency and bandwidth of the envelope amplifier and the RF PA, the AM–AM and AM–PM distortions of the RF PA, and the time alignment of the envelope and phase signals—all of which are critical to the efficiency and linearity of the transmitter. As a modern derivative of the Kahn EER approach, polar modulation generates the modulation envelope and phase components in the digital domain. Therefore, digital signal processing can significantly improve the linearity of the transmitter at the expense of increased system complexity.

Since an injection-locked oscillator (ILO) tends to follow the frequency variations of an injection signal, high-gain amplification of a frequency-modulated or a phase-modulated signal using an ILO has become a popular application [17]–[19]. Based on an injection-locking approach, switch-mode PAs have been designed recently to reduce the stringent input driving requirements, resulting in a high gain and high power-added efficiency (PAE) [20]–[22]. However, the amplitude-limiting nature of an oscillator confines most applications to amplification of constant envelope modulation signals [22], [23]. For nonconstant envelope modulation signals, applying a supply modulation scheme to an ILO provides a feasible solution [24]. In [24], a pulse-width modulated (PWM) envelope was applied to the gate bias of an ILO to switch it on and off. However, this architecture requires a high-selectivity bandpass

Manuscript received July 11, 2012; revised September 24, 2012; accepted September 25, 2012. Date of publication November 15, 2012; date of current version December 13, 2012. This work was supported in part by the National Science Council, Taiwan, under Grant 100-2221-E-110-081-MY3, Grant 100-2221-E-110-082-MY3, and Grant 101-2622-E-110-005-CC3. This paper is an expanded paper from the IEEE MTT-S International Microwave Symposium, Montreal, QC, Canada, June 17–22, 2012.

C.-T. Chen is with MediaTek Inc., Hsinchu, 30078, Taiwan (e-mail: D963010023@student.nsysu.edu.tw).

T.-S. Horng is with the Department of Electrical Engineering, National Sun Yat-Sen University, Kaohsiung 804, Taiwan (e-mail: jason@ee.nsysu.edu.tw).

K.-C. Peng is with the Department of Computer and Communication Engineering, National Kaohsiung First University of Science and Technology, Kaohsiung 811, Taiwan (e-mail: peterpkg@ccms.nkfust.edu.tw).

C.-J. Li is with the Department of Electronic Engineering, National Taipei University of Technology, Taipei 106, Taiwan (e-mail: chnjung@ntut.edu.tw).

Color versions of one or more of the figures in this paper are available online at http://ieeexplore.ieee.org.

Digital Object Identifier 10.1109/TMTT.2012.2223712

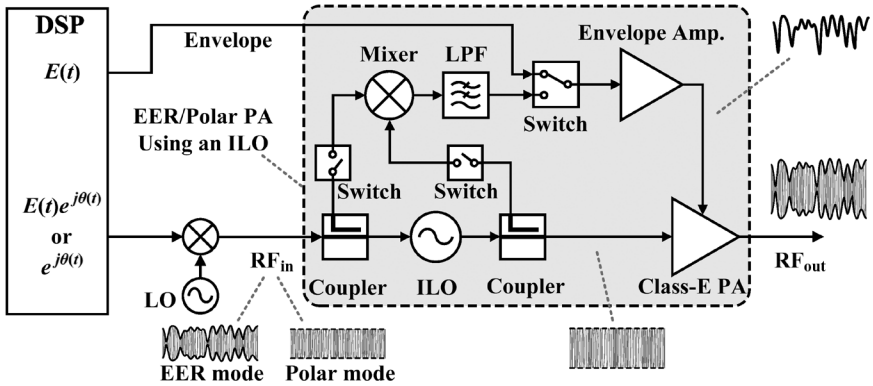

Fig. 1. Block diagram of the proposed EER/polar transmitter using an ILO.

filter for restoring an envelope signal at the transmitter output. Moreover, the applicable modulation bandwidth is limited by the transient response of an ILO from switch-off to switch-on and the switching period of PWM.

This paper presents a novel EER/polar dual-mode transmitter using ILOs. By combining the approaches of EER/polar modulation and injection locking, effectiveness of the implemented transmitter is demonstrated for delivering WCDMA and EDGE signals with a high gain and high efficiency. This paper has substantially expanded the earlier work [25] to improve the linearity of the proposed EER transmitter with static digital predistortion (DPD). Additionally, an extension to a polar transmitter based on the developed technology was presented as a promising alternative with enhanced linearity.

II. System Analysis

A. Transmitter Architecture

Fig. 1 shows the block diagram of the proposed EER/polar transmitter using an ILO. When the transmitter operates in the EER mode, an ILO that is combined with a mixer and a low-pass filter (LPF) can separate an injection signal with complex modulation into an envelope signal and a phase-modulated RF signal, subsequently dispensing with an envelope detector and a limiter required in a conventional EER transmitter. The phase-modulated RF signal is then amplified efficiently by a class-E PA, while the envelope signal is reconstructed at the PA output by modulating the supply voltage of the PA. As in the polar mode, the necessary envelope and phase signals are generated in the baseband digital signal processor (DSP). Instead, the ILO is injected with a constant envelope, phase-modulated RF signal and the PA is supply modulated with an envelope signal directly from the DSP. The mixer and LPF for envelope extraction are thus bypassed in this mode.

B. Separation of Envelope and Phase Signals

The EER mode and polar mode differ mainly in that an ILO is responsible for separating envelope and phase signals for the former, while not for the latter. System analysis of the proposed transmitter considers the EER mode first. Similar results for polar mode can then be derived simply by omitting the mixer and the LPF in the system shown in Fig. 1. Fig. 2 displays the system model of the proposed transmitter in an EER operation, where the mixer is treated as an ideal multiplier. The

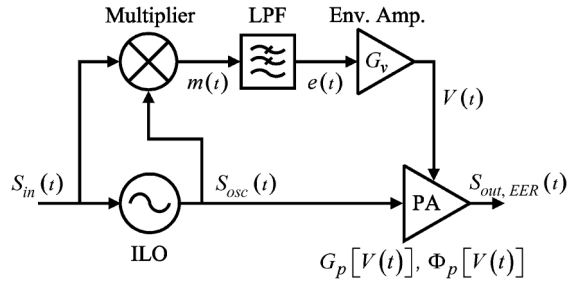

Fig. 2. System model of the proposed transmitter in an EER operation.

complex-modulated input signal $S_{in}(t)$ can be expressed with Cartesian coordinate components $V_I(t)$ and $V_Q(t)$ or polar coordinate components $E(t)$ and $\theta(t)$ as

$$\begin{aligned} S_{in}(t) &= V_I(t)\cos(\omega_c t) + V_Q(t)\sin(\omega_c t) \\ &= E(t)\cos\left[\omega_c t + \theta(t)\right] \end{aligned} \tag{1}$$

where ω_c denotes the RF carrier frequency. The envelope signal $E(t)$ and the phase signal $\theta(t)$ correlate with the in-phase signal $V_I(t)$ and quadrature signal $V_Q(t)$ as

$$E(t) = \sqrt{V_I(t)^2 + V_Q(t)^2} \tag{2}$$

$$\theta(t) = \arctan\left[\frac{V_Q(t)}{V_I(t)}\right]. \tag{3}$$

The injection signal $S_{in}(t)$ has an instantaneous frequency $\omega_{in}(t)$, written as

$$\omega_{in}(t) = \omega_c + \frac{d\theta(t)}{dt} = \omega_c + \omega_m(t) \tag{4}$$

where $\omega_m(t)$ represents the frequency modulation (FM) component of $S_{in}(t)$. With reference to previous studies on the injection-locking phenomena in oscillators [17]–[19], [26]–[28], the instantaneous frequency of the resulting oscillator output signal under injection is given as

$$\begin{aligned} \omega_o(t) &= \omega_{\text{in}}(t) + \frac{d\alpha(t)}{dt} \\ &= \omega_{\text{osc}}(t) - \omega_{LR}(t)\cdot\sin\alpha(t) \end{aligned} \tag{5}$$

where

$$\omega_{LR}(t) = \frac{\omega_{\text{osc}}(t)}{2Q}\cdot\frac{E(t)}{E_{\text{osc}}} \tag{6}$$

is interpreted as the locking range of the oscillator under injection, $\alpha(t)$ denotes the instantaneous angle between the injection signal and the inherent oscillation signal, and $\omega_{\rm osc}(t)$, $E_{\rm osc}$, and Q refer to the inherent oscillation frequency of the oscillator, the oscillation amplitude, and the quality factor of its tank circuit, respectively. Equation (5) indicates that the composite frequency of an oscillator under injection is a sum of its free-running frequency $\omega_{\rm osc}(t)$ and a disturbing frequency modulation equal to $\omega_{\rm LR}(t)\cdot\sin\alpha(t)$, in which $\omega_{\rm LR}(t)$ and $\alpha(t)$ are regarded as the amplitude-to-frequency modulation (AM–FM) and phase-to-frequency modulation (PM–FM) mechanisms resulting from the injection signal, respectively. When an oscillator is synchronized with the injected modulation signal, the instantaneous frequency of the oscillator tends to follow the frequency variations of the modulation (i.e. FM). However, the AM–FM and PM–FM effects degrade the reproduction of the FM of the injection signal at the ILO output.

Assume that the ILO is synchronized with $S_{\rm in}(t)$ and the distortion due to AM-FM and PM-FM is slight. The ILO output $S_{\rm osc}(t)$ can thus be approximated as

$$S_{\rm osc}(t)\approx E_{\rm osc}\cos\left[\omega_c(t-\tau)+\int\omega_m(t-\tau)dt\right] \tag{7}$$

where τ denotes the effective lock-in time that is introduced by the ILO. The mixer output $m(t)$ is found as

$$\begin{aligned} m(t)\propto S_{\rm in}(t)\cdot S_{\rm osc}(t) =&E(t)\cos\left[\omega_c t+\theta(t)\right]\\ &\cdot E_{\rm osc}\cos\left[\omega_c(t-\tau)+\int\omega_m(t-\tau)dt\right]. \end{aligned} \tag{8}$$

When a zero phase shift condition is applied to (8), that is,

$$\omega_c\cdot\tau=k\cdot 360^\circ,\quad k=0,1,2\ldots \tag{9}$$

and the second-order term of (8) is filtered out by an ideal LPF, the filter output $e(t)$ can be derived as

$$e(t)\propto E(t)E_{osc}\cos\left[\omega_m(t)\tau\right]\approx E_{osc}E(t). \tag{10}$$

Here, τ is assumed to be small so that the approximation in (10) applies. Equations (10) and (7) represent the envelope signal and the phase-modulated RF signal, respectively, that are extracted from the input complex-modulated RF signal for subsequent separate amplification. Importantly, the proposed transmitter is simpler and has a higher gain than the conventional EER scheme. Moreover, the effective lock-in time of the ILO potentially alleviates the need for a bulky delay line in a conventional EER transmitter, thus favoring the integration of an EER transmitter in a single chip.

C. Recombination of Envelope and Phase Signals

In the following stage, the envelope signal and the phase-modulated RF signal are amplified by an envelope amplifier and a class-E PA, respectively; meanwhile the envelope modulation is reconstructed at the PA output by varying the supply voltage of the PA, as shown in Fig. 2. On assumptions that the inherent FM of a free-running oscillator caused by phase noise perturbation is far smaller than its carrier frequency and the oscillator is synchronized to a narrowband modulation injection, the following approximations are valid for this analysis:

$$\omega_{\rm osc}(t)\approx\omega_{\rm osc} \tag{11}$$

$$\omega_{\rm in}(t)\approx\omega_c. \tag{12}$$

Therefore, (5) can be rewritten as

$$\omega_o(t)\approx\omega_{\rm in}(t)-\frac{\omega_{\rm osc}}{2Q}\cdot\frac{E(t)}{E_{\rm osc}}\cdot\sin\alpha(t)+\Delta\omega_{\rm osc} \tag{13}$$

where

$$\Delta\omega_{\rm osc}=\omega_{\rm osc}-\omega_c. \tag{14}$$

Integrating both sides of (13) leads to the instantaneous phase of the ILO as

$$\begin{aligned} \phi_o(t)=&\int\omega_o(t)dt\\ \approx&\int\omega_{\rm in}(t)dt-\int\frac{\omega_{\rm osc}}{2Q}\cdot\frac{E(t)}{E_{osc}}\cdot\sin\alpha(t)dt+\int\Delta\omega_{\rm osc}dt\\ =&\omega_c t+\theta(t)+\phi_0-\frac{\omega_{\rm osc}}{2QE_{\rm osc}}\int E(t)\cdot\sin\alpha(t)dt+\Delta\omega_{\rm osc}t\\ =&\omega_c t+\theta(t)+\phi_0-\phi_{\rm inj}(t)+\phi_{\rm osc}(t) \end{aligned} \tag{15}$$

where ϕ_0, $\phi_{\rm inj}(t)$, and $\phi_{\rm osc}(t)$ refer to an initial oscillation phase, the instantaneous phase response due to injection, and the instantaneous oscillation phase, respectively. Next, consider a time-alignment condition, in which no differential delay occurs between the envelope and phase paths. Therefore, the output signal of the transmitter in EER mode, $S_{\rm out,EER}(t)$, can be expressed as

$$\begin{aligned} S_{\rm out,EER}(t)=&V(t)\cdot G_p\left[V(t)\right]\cdot E_{\rm osc}\cdot\cos\left\{\phi_o(t)+\Phi_p\left[V(t)\right]\right\}\\ =&G_v\cdot e(t)\cdot G_p\left[V(t)\right]\cdot E_{\rm osc}\\ &\cdot\cos\left\{\omega_c t+\theta(t)+\phi_0-\phi_{\rm inj}(t)+\phi_{\rm osc}(t)\right.\\ &\left.+\Phi_p\left[V(t)\right]\right\} \end{aligned} \tag{16}$$

where G_v denotes the gain of the envelope amplifier, and G_p and Φ_p represent the AM–AM and AM–PM distortions of the class-E PA, respectively.

For a polar mode operation, since the oscillator is injected with a phase-modulated RF signal, which has a constant envelope, the resulting oscillator output signal under injection is thus free of AM–FM distortion. The instantaneous phase response of the ILO due to injection is modified as

$$\phi'_{\rm inj}(t)=\frac{\omega_{\rm osc}E_i}{2QE_{\rm osc}}\int\sin\alpha(t)dt \tag{17}$$

where E_i denotes the constant amplitude level of the injection signal. Therefore, the output signal of the transmitter in polar mode $S_{\rm out,Polar}(t)$ can be expressed as

$$\begin{aligned} S_{\rm out,Polar}(t)=&G_v\cdot E(t)\cdot G_p\left[V(t)\right]\cdot E_{\rm osc}\\ &\cdot\cos\left\{\omega_c t+\theta(t)+\phi_0-\phi'_{\rm inj}(t)\right.\\ &\left.+\phi_{\rm osc}(t)+\Phi_p\left[V(t)\right]\right\}. \end{aligned} \tag{18}$$

Notably, the supply-modulating signal is the envelope signal from DSP, $E(t)$, rather than $e(t)$ in (16).

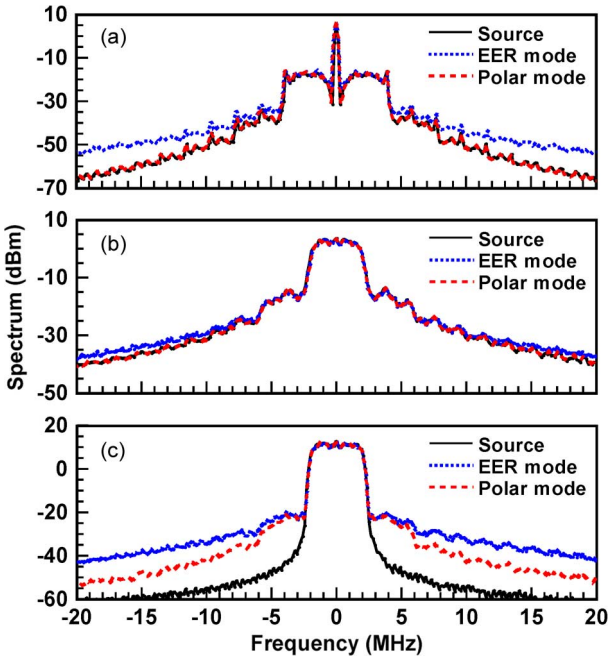

Fig. 3. Spectra of (a) envelope, (b) phase, and (c) reconstructed complex signals of the proposed EER/polar transmitter compared with an ideal WCDMA signal source.

Based on the above analysis, Fig. 3(c) depicts the simulated spectra of the reconstructed WCDMA complex signal at the transmitter output together with its envelope and phase components in Fig. 3(a) and (b), respectively. As derived previously, the extracted envelope exhibits slight distortion during separation of the envelope and phase signals. The phase spectrum of the EER mode also reveals a higher distortion level than that of polar mode due to AM–FM effect. Consequently, as is expected, the proposed transmitter has a higher linearity in the polar mode than in the EER mode.

III. System Front-End Module Implementation

A 1.95-GHz prototype transmitter is constructed to validate the proposed EER/polar transmitter using ILOs. The transmitter module consists of a class-E PA, a voltage-controlled oscillator (VCO) with an injection port, an envelope amplifier, and other commercially available discrete components, including couplers, a mixer with a conversion loss of 4.5 dB, and an LPF with a cutoff frequency of 30 MHz. Details of the circuitry are provided as follows.

A. Class-E Power Amplifier

For high-efficiency switch-mode PAs, the class-E PA is a popular topology because of its design simplicity in the load network. The classic class-E condition sets the voltage across the switch and its first derivative both equal to zero at the instant of switch-on in order to attain a theoretical 100% dc-to-RF efficiency [29]. In practice, however, several nonidealities degrade the efficiency. Fig. 4 schematically depicts the 1.95-GHz class-E PA developed in this work. The power transistor is designed in 0.15-μm GaAs pHEMT technology and treated as a voltage-controlled switch with a finite switch-on resistance and finite switch-off resistance to account for transistor loss [30]. Additionally, the finite dc-feed inductance (L_D), the bondwire inductance (L_B), and the parasitic transistor output capacitance $(C_{\rm ds})$ are also considered in the solution for maximum efficiency. Finally, the input matching network (C_1 and C_2) and the output load network (C_S, L_S, and L_1) are used to realize maximum power transfer and optimal class-E load impedance, respectively.

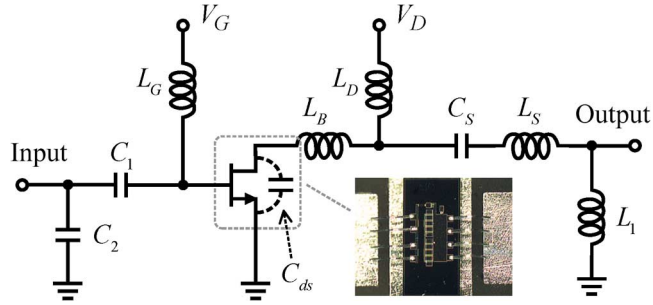

Fig. 4. Simplified schematic of the implemented Class-E PA.

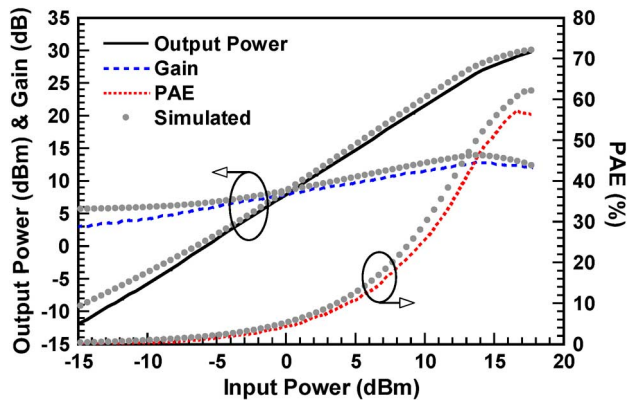

Fig. 5. CW measurements of the 1.95-GHz Class-E PA. ($V_G = -1.2$ V; $V_D = 5.5$ V.).

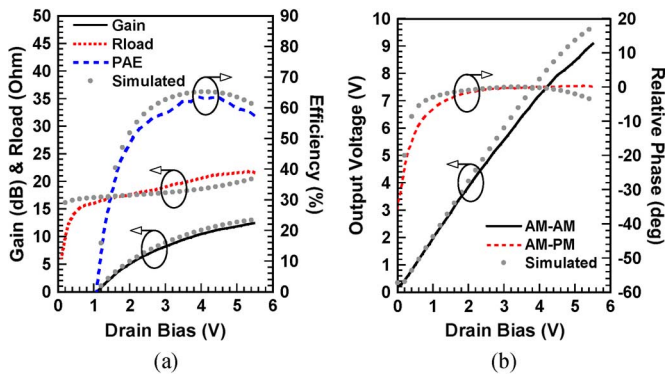

Fig. 6. CW measurements of the 1.95-GHz Class-E PA in an EER/polar operation by sweeping PA drain voltage. The input power is fixed at 16.6 dBm.. (a) PAE, gain, and impedance looking into the drain of the PA. (b) AM–AM and AM–PM of the PA.

Fig. 5 plots the measured and simulated results of the class-E PA with a drain supply voltage (V_D) of 5.5 V in a continuous-wave (CW) test. The PA has a maximum PAE of 57% and a power gain of 12.5 dB at an input power of 16.6 dBm. Fig. 6(a) shows the CW characteristics of the PA in an EER/polar operation by sweeping the PA drain voltage; meanwhile, the input power is fixed to 16.6 dBm for optimal PAE. The impedance

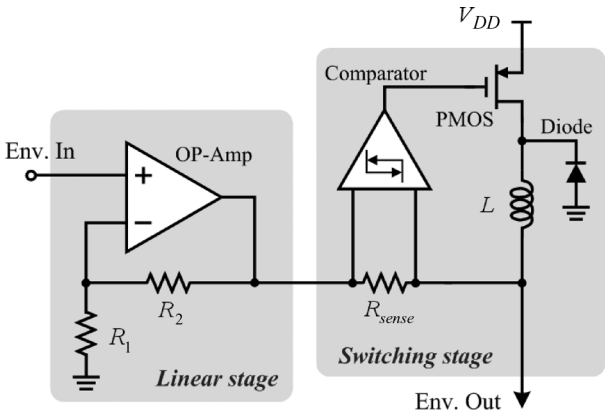

Fig. 7. Simplified schematic of the implemented discrete split-band envelope amplifier.

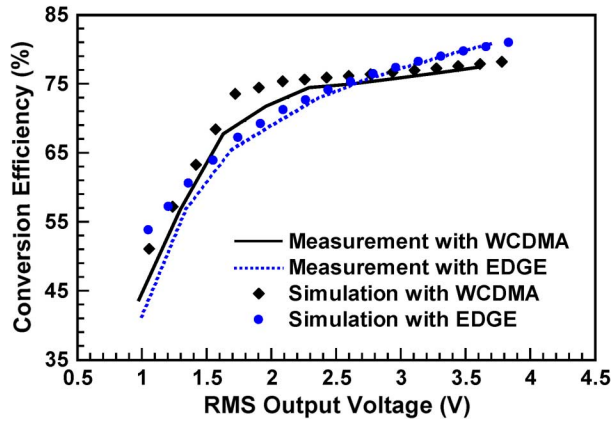

Fig. 8. Measured and simulated conversion efficiency of the envelope amplifier versus rms output voltage while delivering envelopes of WCDMA and EDGE signals with a load resistance of 20 Ω.

looking into the drain of the PA, which is equivalent to the load impedance (R_L) of the envelope amplifier, changes from 16 to 21 Ω when the drain voltage increases from 1 to 5.5 V. Fig. 6(b) shows the corresponding AM–AM and AM–PM characteristics of the PA. The PA generally exhibits a stronger nonlinearity at a low supply voltage than at a high supply voltage. The feedthrough effect also introduces distortion in signals with envelope zero crossings [5].

B. Envelope Amplifier

As is well known, the overall efficiency of an EER/polar transmitter is the product of the efficiencies of the envelope amplifier and the power amplifier on the assumption that the power consumption of other devices in the transmitter is negligible. A high-efficiency envelope amplifier design is as important as a high-efficiency class-E PA design. Furthermore, the nonlinear transformation from the Cartesian coordinate to the polar coordinate results in substantially wider bandwidths of the envelope and phase signals than that of the baseband complex signal [10]. A conventional dc–dc converter is no longer applicable for wideband applications, such as WCDMA signals. This work designs a split-band envelope amplifier that comprises a wideband linear stage and an efficient narrowband switching stage to achieve high linearity and efficiency simultaneously [10], [31]. Fig. 7 schematically depicts the simplified discrete circuit of the envelope amplifier. The operational amplifier (op-amp) has a 3-dB bandwidth of 220 MHz, and the comparator has a hysteresis voltage of 7 mV. Fig. 8 illustrates the conversion efficiencies of the envelope amplifier at various root-mean-square (rms) output voltages while delivering the envelope of WCDMA and EDGE signals with a load resistance of 20 Ω. The efficiency is over 60% for an rms output voltage larger than 1.5 V. Due to the static power consumption of the op-amp, the efficiency generally degrades with a decreasing rms output voltage.

C. Injection-Locked Oscillator

Fig. 9 shows the simplified schematic of the implemented discrete VCO with an injection port. To drive the PA properly, the VCO has an output power of 17.5 dBm at 1.95 GHz and covers the frequency from 1.91 to 2.02 GHz, with a tuning voltage ranging from 0 to 6 V. The measured dc-to-RF conversion efficiency at 1.95 GHz is 43%. Fig. 10 plots the minimum

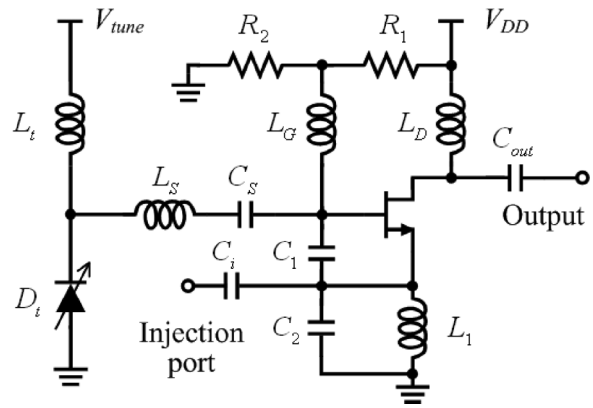

Fig. 9. Simplified schematic of the implemented discrete VCO with an injection port.

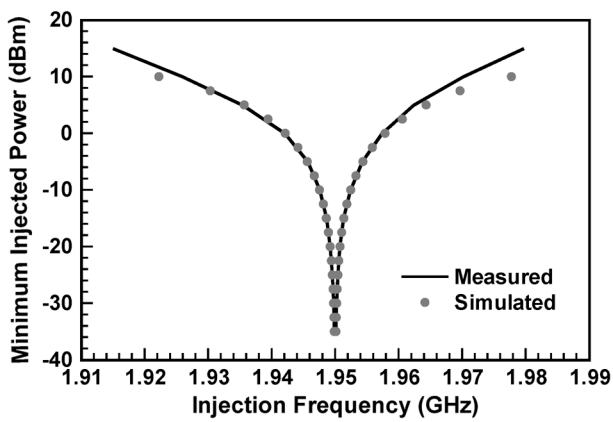

Fig. 10. Measured and simulated injection-locking characteristic of the VCO.

injected power required to lock the VCO at various injection frequencies. According to the derivation by Huntoon [17], the distortion of an ILO that acts as a synchronous amplifier can be negligible if its locking range is at least twice larger than the peak frequency deviation of the frequency-modulated signal to be amplified. Consequently, designing an appropriate input power of the EER/polar transmitter is vital to the linearity of the system, as illustrated by simulation and measurement results in

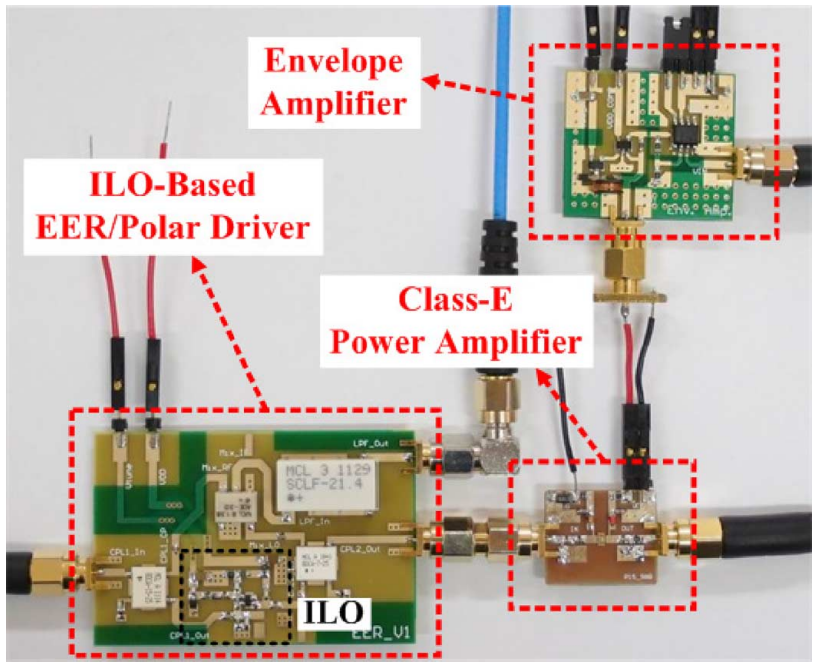

Fig. 11. Photograph of the implemented EER/polar transmitter front-end module.

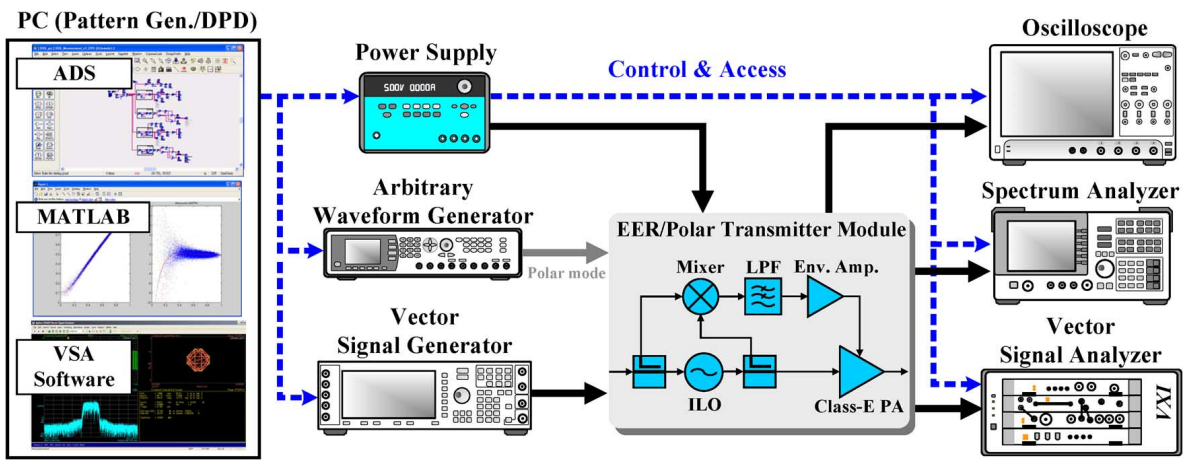

Fig. 12. Measurement setup of the proposed EER/polar transmitter.

Section IV. Fig. 11 shows the photograph of the implemented transmitter module by integrating the above mentioned circuits.

IV. System Measurements

Fig. 12 shows the measurement setup of the proposed transmitter. Effectiveness of the prototype transmitter is demonstrated with WCDMA and EDGE signals in both EER and polar modes. This work attempts to improve the modulation accuracy of the transmitter by using lookup-table (LUT)-based DPD. The predistorter has a polar configuration. The AM LUT and the PM LUT are constructed by characterizing the AM–AM and AM–PM distortions of the transmitter, respectively [30]. WCDMA and EDGE baseband signals that incorporate the DPD function are then generated using Agilent's Advanced Design System (ADS) and MATLAB software. Notably, the conversion between Cartesian and polar coordinates is carried out by a coordinate rotation digital computer (CORDIC) in the DSP, as similarly done in [7] and [30].

Next, the generated envelope and baseband signals are then loaded into an arbitrary waveform generator (AWG) and a vector signal generator which is also used as an RF modulator, respectively. The transmitter output signals are received by a spectrum analyzer and a vector signal analyzer for signal quality analysis. Additionally, a high-speed digitizing oscilloscope captures the instantaneous drain supply voltage of the PA and the input and output RF signals of the transmitter to observe the time alignment between the envelope and phase paths. Finally, the measuring instruments in the testbed are triggered in synchronization and accessed using a computer.

A. WCDMA

A WCDMA signal based on a hybrid phase-shift keying (HPSK) modulation scheme is used to test the proposed transmitter. The signal has a channel bandwidth of 5 MHz and a peak-to-average power ratio (PAPR) of 3.4 dB [32]. In the proposed architecture, differential delay is compensated for by

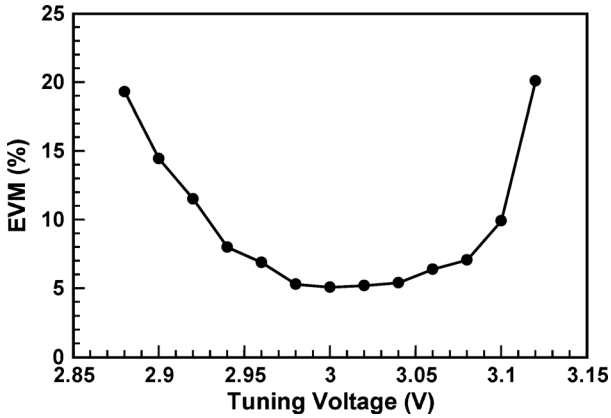

Fig. 13. Measured EVM versus tuning voltage of the ILO.

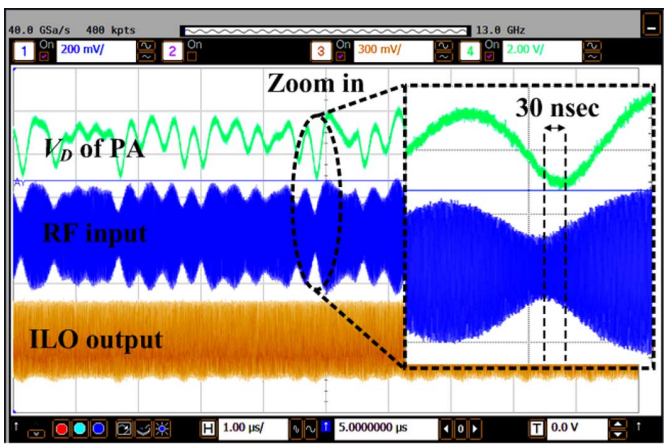

Fig. 14. Time-domain waveforms of the drain voltage of the PA, input RF signal, and ILO output signal.

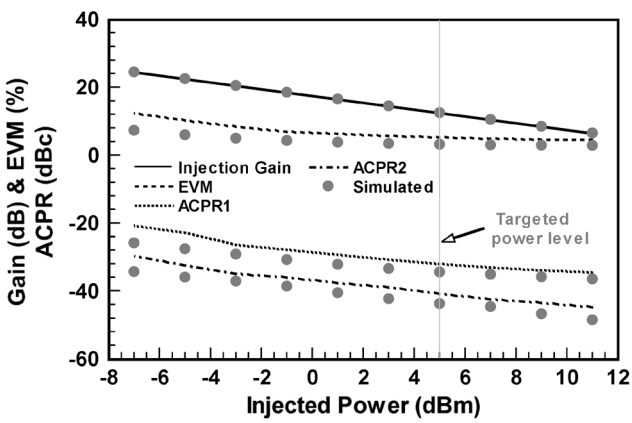

Fig. 15. Measured and simulated injection gain, EVM, and ACPR versus injected power for the proposed EER transmitter with WCDMA input signals.

using the effective lock-in time introduced by the ILO, which is adjustable by tuning the inherent oscillation frequency [28]. With an injected WCDMA power of 5 dBm, Fig. 13 shows the measured EVM versus the tuning voltage of the ILO. In a limited range of tuning voltage, EVM is optimized at a tuning voltage of 3 V. Beyond this range, the modulation quality is degraded severely because injection pulling occurs. Fig. 14 shows the time-domain waveforms of the drain voltage of the

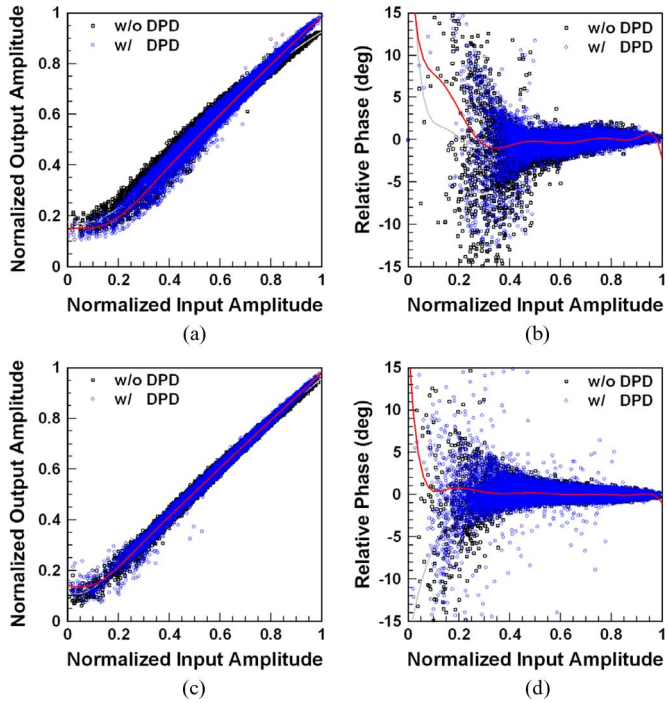

Fig. 16. Measured AM–AM and AM–PM characteristics of the proposed EER/polar transmitter with WCDMA input signals. (a) AM–AM for the EER mode. (b) AM–PM for the EER mode. (c) AM–AM for the polar mode. (d) AM–PM for the polar mode.

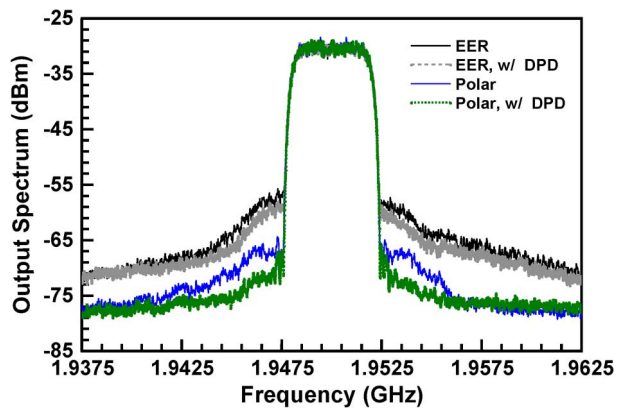

Fig. 17. Measured output spectra of the proposed EER/polar transmitter with WCDMA input signals.

PA, the input RF signal and the ILO output signal captured by an oscilloscope under time-alignment condition. Notably, a 30-ns delay difference between the drain voltage of the PA and the input RF signal is observed. This finding implies that the ILO contributes an effective lock-in time of 30 ns to the RF path in order to compensate for the delay mismatch. Measurement results verify the feasibility of using an ILO as a delay element for delay compensation, as described in Section II.

To demonstrate the design considerations when determining the injected power of the proposed transmitter, Fig. 15 shows the relations of the injected power to the injection gain, EVM and ACPR. The injection gain is defined as the ratio of the ILO output power to the injected power. According to the measurement and simulation results, a higher injected power implies a better linearity, i.e. a lower EVM and a lower ACPR, yet

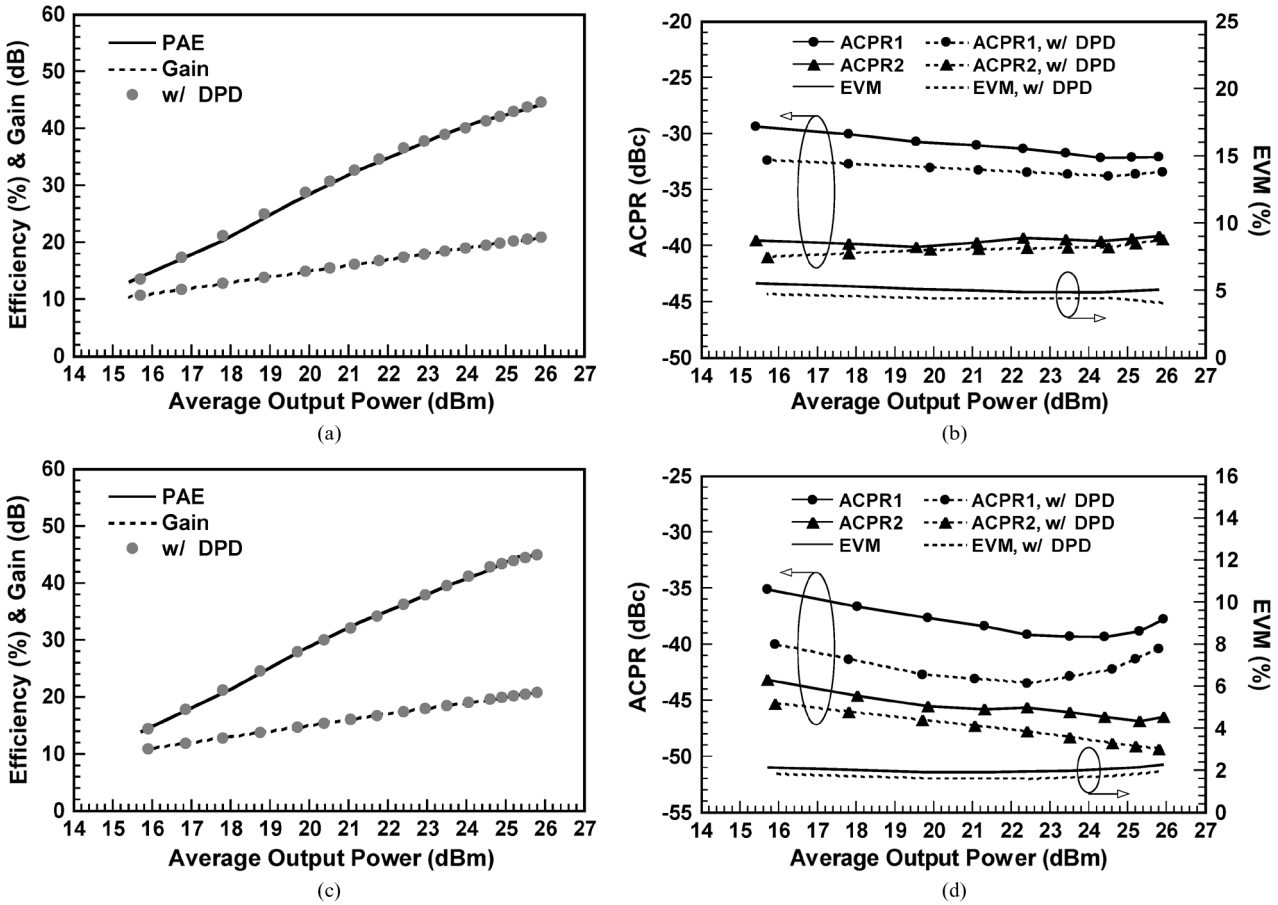

Fig. 18. Measured efficiency, gain, ACPR, and EVM of the proposed EER/polar transmitter with WCDMA input signals. (a) Gain and efficiency for the EER mode. (b) ACPR and EVM for the EER mode. (c) Gain and efficiency for the polar mode. (d) ACPR and EVM for the polar mode.

a lower injection gain. Thus, an inherent tradeoff occurs between gain and linearity. At the designed injected WCDMA power of 5 dBm, the injection gain and EVM of the transmitter are 12.5 dB and 5.1%, respectively. Fig. 16(a) and (b) display the measured AM–AM and AM–PM characteristics of the transmitter before and after DPD for the EER mode, while Fig. 16(c) and (d) show the results for the polar mode. Notably, the injected power for polar mode is 5 dBm as well for comparison purposes. These figures reveal that the AM–FM effect of the ILO deteriorates the FM of the injected signal, subsequently resulting in wider distributions of AM–AM and AM–PM in the EER mode than that in the polar mode. This effect is particularly evident when the envelope level is close to zero crossing, causing an invalid injection-locking condition. The static DPD mainly compensates for the AM–AM and AM-PM distortions of the class-E PA. Therefore, the linearity of the proposed transmitter markedly improves in the polar mode because of the constant envelope modulation signal injection, i.e. without the AM–FM effect. Fig. 17 compares the transmitter output spectra before and after DPD for both modes at an average output power of 22.4 dBm.

Fig. 18(a) depicts the measured average efficiency and gain of the transmitter in the EER mode. The PAE of the EER transmitter includes the efficiencies of the ILO, the envelope amplifier and the class-E PA. The transmitter achieves a peak PAE of 44% and a gain of 20.8 dB at the maximum average output power of 25.8 dBm. Fig. 18(b) shows the measured ACPR and EVM for the EER mode. With DPD, ACPR1 can barely meet the required specification of −33 dBc in the measured average output power ranging from 15.5 to 25.8 dBm. Meanwhile, ACPR2 fails to comply with the required specification of −43 dBc. The EVMs vary from 4% to 4.7% after DPD in the identical power range. Fig. 18(c) and (d) illustrates the same measurements of the transmitter in the polar mode.

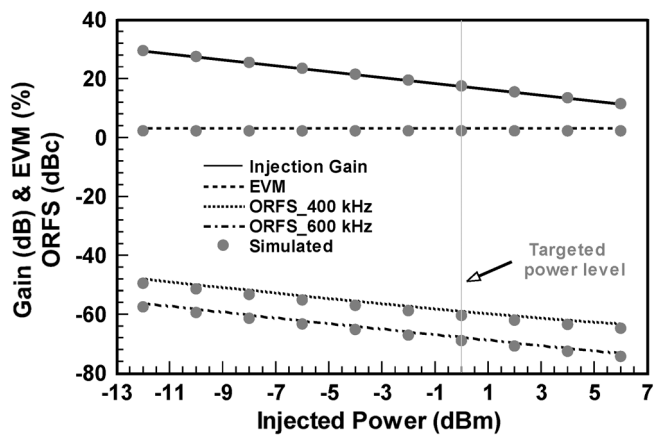

Fig. 19. Measured and simulated injection gain, EVM, and ORFS versus injected power for the proposed EER transmitter with EDGE input signals.

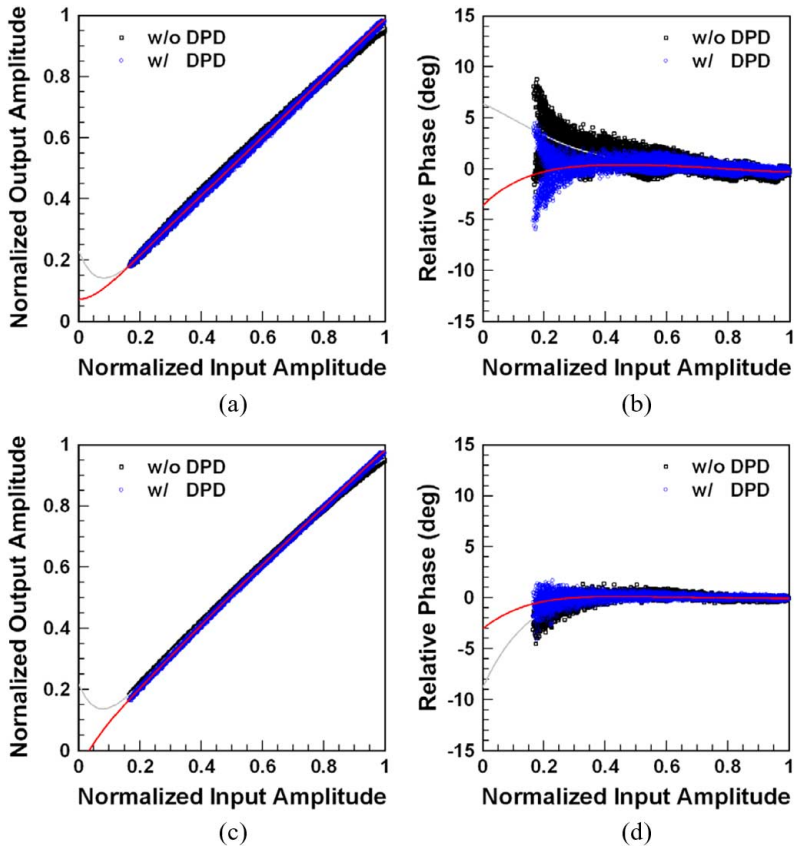

Fig. 20. Measured AM–AM and AM–PM characteristics of the proposed EER/polar transmitter with EDGE input signals. (a) AM–AM for the EER mode. (b) AM–PM for the EER mode. (c) AM–AM for the polar mode. (d) AM–PM for the polar mode.

Although both modes have similar performance in efficiency and gain, polar mode exhibits better linearity than EER mode. According to Fig. 18(d), both ACPR1 and ACPR2 comply with the requirements of WCDMA with or without DPD. Additionally, the EVMs are below 2% after DPD in the measured average output power range.

B. EDGE

The ILO-based transmitter is also tested on an EDGE signal with eight phase-shift keying (8PSK) modulation. The signal has a symbol rate of 270.833 kHz and a PAPR of 3.4 dB [7]. Fig. 19 shows the injection gain, EVM, and EDGE output RF spectrum (ORFS) versus the injected power when the proposed transmitter operates in the EER mode. At the designed injected EDGE power of 0 dBm, the injection gain and EVM are 17.5 dB and 3.12%, respectively. Fig. 20(a) and (b) shows the measured AM–AM and AM–PM characteristics of the proposed transmitter before and after DPD for the EER mode, while Fig. 20(c) and (d) shows the results for the polar mode. Again, the AM–FM effect of the ILO is observed in the EER mode, resulting in a worse AM–AM and AM–PM for the EER mode than that for the polar mode. However, the distortion caused by the AM–FM effect is largely reduced, in comparison with the WCDMA case. This difference is because an EDGE signal has a smaller channel bandwidth than a WCDMA signal; in addition, zero crossing is avoided for 8PSK modulation using a rotation of $3\pi/8$ radians. Fig. 21 compares the transmitter

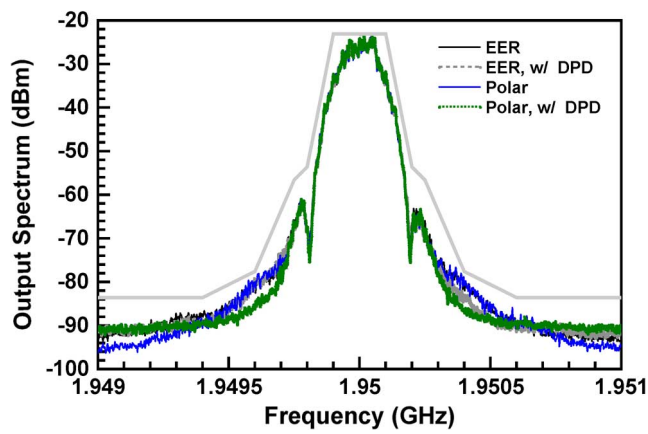

Fig. 21. Measured output spectra of the proposed EER/polar transmitter with EDGE input signals.

output spectra before and after DPD for both modes at an average output power of 22 dBm.

In a similar manner, Fig. 22(a) shows the measured average efficiency and gain of the transmitter versus the average output power in the EER mode. The transmitter achieves a peak PAE of 48.7% and a gain of 26.6 dB at the maximum average output power of 26.6 dBm. Fig. 22(b) shows the measured EDGE ORFS in decibels relative to the carrier (dBc) at 400- and 600-kHz offset and EVM for the EER mode. With DPD, the spectra due to modulation comply with the EDGE spectrum mask specification of -54 dBc at 400-kHz offset and -60 dBc

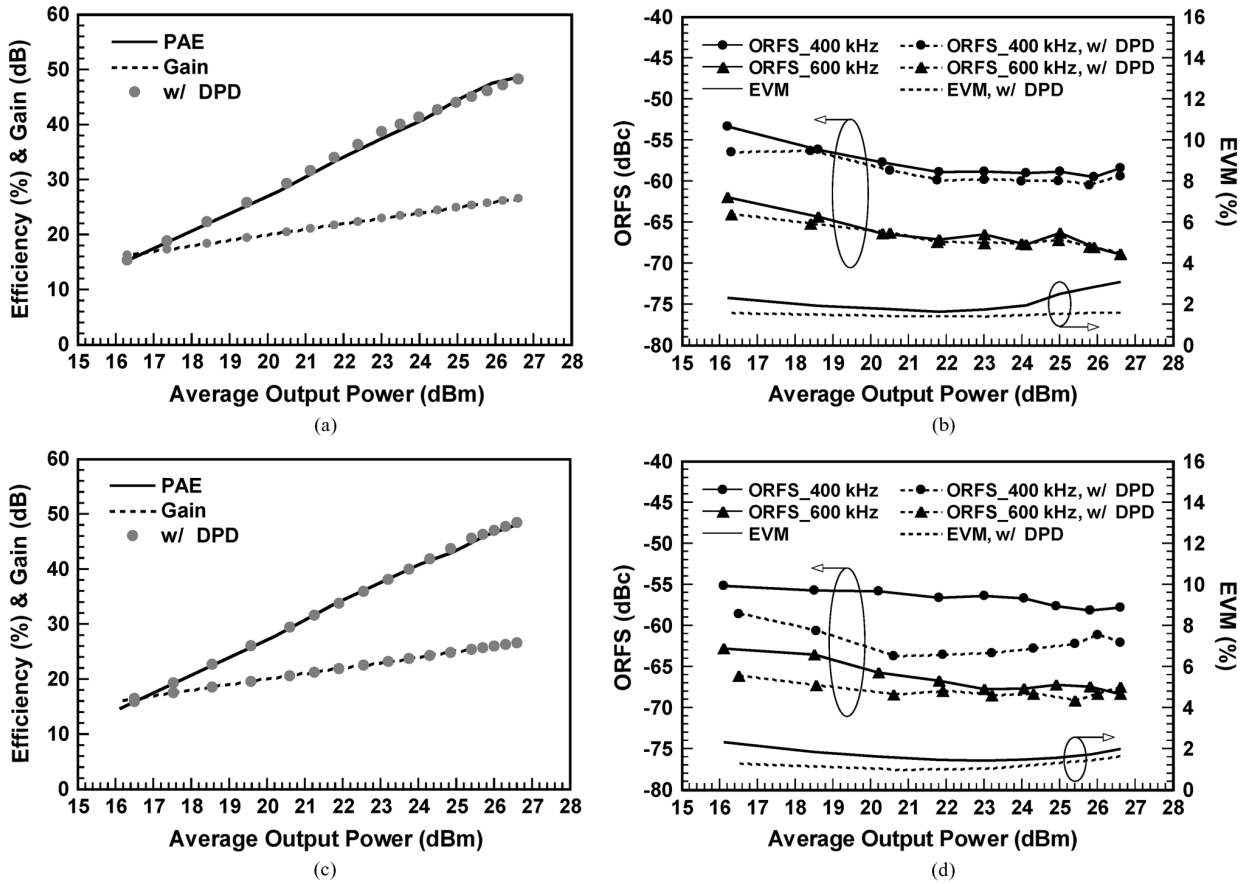

Fig. 22. Measured efficiency, gain, ORFS, and EVM of the proposed EER/polar transmitter with EDGE input signals. (a) Gain and efficiency for the EER mode. (b) ORFS and EVM for the EER mode. (c) Gain and efficiency for the polar mode. (d) ORFS and EVM for the polar mode.

TABLE I
COMPARISON OF THIS WORK WITH RECENT WORKS ON EER/POLAR/ET TRANSMITTERS

Reference	Efficiency Enhancement Technique	Amplification Topology	Freq. (MHz)	Modulation	Bandwidth	Gain (dB)	Pout (dBm)	Overall PAE	EVM	PD [b]
[7]	Polar	Two-stage driver plus class-E PA	1750	EDGE	384 kHz	–	23.8	22%	1.69%	Yes
[9]	Pulse modulated polar	Driver plus class-C PA	836.5	WCDMA EDGE	3.84 MHz 384 kHz	22.7 23	25 26	41.2% 45.5%	– 1.9 %	No
[10]	Hybrid EER	Class-E PA	2400	WLAN 64QAM	20 MHz	6.5	19	28%	2.8%	Yes
[13]	Envelope tracking with envelope shaping	Driver plus class-AB/F PA	1880	WCDMA EDGE	3.84 MHz 384 kHz	27.8 29.4	29 27.8	46% 45.3%	2.98% –	Yes
[14]	Envelope tracking	Self-biased cascade PA	1750	LTE 16QAM	5 MHz	19.5	24.2	43%	4.8%	No
[22]	PWM digitized polar with injection locking	Driver plus ILPA	820	GSM	270.833 kHz	–	28	–	–	No
[24]	PWM digitized polar with injection locking	Class-F ILO	1900	OQPSK	< 800 kHz [a]	–	–	–	3.1%	No
This Work	EER with injection locking	ILO plus class-E PA	1950	WCDMA EDGE	3.84 MHz 384 kHz	20.8 26.6	25.8 26.6	44% 48.7%	4.02% 1.6%	Yes
This Work	Polar with injection locking	ILO plus class-E PA	1950	WCDMA EDGE	3.84 MHz 384 kHz	20.8 26.6	25.8 26.6	44.9% 48.1%	1.96% 1.66%	Yes

[a] With a PWM switching frequency of 8 MHz.

[b] Predistortion.

at 600-kHz offset in the measured average output power ranging from 16.3 to 26.6 dBm. The EVMs vary from 1.4% to 1.6% after DPD in the same power range. Fig. 22(c) and (d) shows the same measurements when the transmitter operates in the polar mode. Both modes perform similarly in efficiency and gain, and the linearity for the polar mode slightly outperforms the linearity for the EER mode.

Above measurement and simulation results with WCDMA and EDGE signals indicate that the linearity of the proposed transmitter depends significantly on the ILO. Additionally,

applying static DPD to linearize the transmitter is generally more effective in the polar mode than in the EER mode. This difference is owing to the inability of the static DPD to fully compensate for the phase perturbation caused by the AM–FM effect of the ILO. Therefore, polar mode operation is favorable for complex modulation schemes with envelope zero crossings, high PAPR, or high data rate. Otherwise, we recommend a more advanced linearization method, e.g., adaptive DPD [32], for the EER mode.

Table I compares this work with other recent works on EER/polar/ET transmitters. Because of injection locking, the ILO can simultaneously serve as a high-gain driver stage and a delay element for differential delay compensation. Therefore, the proposed transmitter has a reduced complexity while achieving a high gain and high efficiency, which are comparable to those of other transmitters.

V. Conclusion

This paper presents a novel EER/polar dual-mode transmitter using ILOs. With characterizations of an ILO under nonconstant envelope modulation injection and a class-E PA in a supply modulation scheme, the operating principles and performance of the proposed transmitter system are derived and analyzed in detail. The implemented 1.95 GHz prototype transmitter is tested with WCDMA and EDGE signals in the EER mode and in the polar mode. The transmitter achieves a gain of 20.8 and 26.6 dB, as well as an overall PAE of 44% and 48.7% at 25.8- and 26.6-dBm average output power for WCDMA and EDGE signals, respectively. The results show that the proposed EER/polar transmitter using ILOs is promising for highly efficient linear amplification, owing to its high gain, high efficiency, and simplicity of system integration.

References

[1] S. C. Cripps, *RF Power Amplifiers for Wireless Communications*, 2nd ed. Norwood, MA: Artech House, 2006.

[2] L. R. Kahn, "Single-sideband transmission by envelope elimination and restoration," *Proc. IRE*, vol. 40, no. 7, pp. 803–806, Jul. 1952.

[3] F. H. Raab, B. E. Sigmon, R. G. Myers, and R. M. Jackson, "L-band transmitter using Kahn EER technique," *IEEE Trans. Microw. Theory Tech.*, vol. 46, no. 12, pp. 2220–2225, Dec. 1998.

[4] D. Su and W. McFarland, "An IC for linearizing RF power amplifiers using envelope elimination and restoration," *IEEE J. Solid-State Circuits*, vol. 33, no. 12, pp. 2252–2258, Dec. 1998.

[5] N. Wang, X. Peng, V. Yousefzadeh, D. Maksimovic, S. Pajic, and Z. Popovic, "Linearity of X-band class-E power amplifiers in EER operation," *IEEE Trans. Microw. Theory Tech.*, vol. 53, no. 3, pp. 1096–1102, Mar. 2005.

[6] D. C. Cox, "Linear amplification with nonlinear components," *IEEE Trans. Commun.*, vol. 22, no. 12, pp. 1942–1945, Dec. 1974.

[7] P. Reynaert and M. S. J. Steyaert, "A 1.75-GHz polar modulated CMOS RF power amplifier for GSM-EDGE," *IEEE J. Solid-State Circuits*, vol. 40, no. 12, pp. 2598–2608, Dec. 2005.

[8] J. N. Kitchen, I. Deligoz, S. Kiaei, and B. Bakkaloglu, "Polar SiGe class E and F amplifiers using switch-mode supply modulation," *IEEE Trans. Microw. Theory Tech.*, vol. 55, no. 5, pp. 845–856, May 2007.

[9] H.-S. Yang, J.-H. Chen, and Y.-J. E. Chen, "A polar transmitter using interleaving pulse modulation for multimode handsets," *IEEE Trans. Microw. Theory Tech.*, vol. 59, no. 8, pp. 2083–2090, Aug. 2011.

[10] F. Wang, D. F. Kimball, J. D. Popp, A. H. Yang, D. Y. C. Lie, P. M. Asbeck, and L. E. Larson, "An improved power-added efficiency 19-dBm hybrid envelope elimination and restoration power amplifier for 802.11g WLAN applications," *IEEE Trans. Microw. Theory Tech.*, vol. 54, no. 12, pp. 4086–4099, Dec. 2006.

[11] C.-J. Li, C.-T. Chen, T.-S. Horng, J.-K. Jau, and J.-Y. Li, "High average-efficiency multimode RF transmitter using a hybrid quadrature polar modulator," *IEEE Trans. Circuits Syst. II, Exp. Briefs*, vol. 55, no. 3, pp. 249–253, Mar. 2008.

[12] G. Hanington, P. Chen, P. M. Asbeck, and L. E. Larson, "High efficiency power amplifier using dynamic power-supply voltage for CDMA applications," *IEEE Trans. Microw. Theory Tech.*, vol. 47, no. 8, pp. 1471–1476, Aug. 1999.

[13] J. Choi, D. Kim, D. Kang, and B. Kim, "A polar transmitter with CMOS programmable hysteretic-controlled hybrid switching supply modulator for multistandard applications," *IEEE Trans. Microw. Theory Tech.*, vol. 57, no. 7, pp. 1675–1686, Jul. 2009.

[14] Y. Li, J. Lopez, P.-H. Wu, W. Hu, R. Wu, and D. Y. C. Lie, "A SiGe envelope-tracking power amplifier with an integrated CMOS envelope modulator for mobile WiMAX/3GPP LTE transmitters," *IEEE Trans. Microw. Theory Tech.*, vol. 59, no. 10, pp. 2525–2536, Oct. 2011.

[15] M. Hassan, L. E. Larson, V. W. Leung, D. F. Kimball, and P. M. Asbeck, "A wideband CMOS/GaAs HBT envelope tracking power amplifier for 4G LTE mobile terminal applications," *IEEE Trans. Microw. Theory Tech.*, vol. 60, no. 5, pp. 1321–1330, May 2011.

[16] T. Sowlati, Y. Greshishchev, and C. A. T. Salama, "Phase-correcting feedback system for Class E power amplifier," *IEEE J. Solid-State Circuits*, vol. 32, no. 4, pp. 544–550, Apr. 1997.

[17] R. D. Huntoon and A. Weiss, "Synchronization of oscillators," *Proc. IRE*, vol. 35, no. 12, pp. 1415–1423, Dec. 1947.

[18] R. C. Mackey, "Injection locking of klystron oscillators," *IRE Trans. Microw. Theory Tech.*, vol. MTT-10, no. 4, pp. 228–235, Jul. 1962.

[19] H. L. Stover and R. C. Shaw, "Injection-locked oscillators as amplifiers for angle-modulated signals," in *G-MTT Int. Symp. Dig.*, 1966, pp. 60–66.

[20] K.-C. Tsai and P. P. Gray, "A 1.9-GHz, 1-W CMOS class-E power amplifier for wireless communications," *IEEE J. Solid-State Circuits*, vol. 34, no. 7, pp. 962–970, Jul. 1999.

[21] H.-S. Oh, T. Song, E. Yoon, and C.-K. Kim, "A power-efficient injection-locked class-E power amplifier for wireless sensor network," *IEEE Microw. Wireless Compon. Lett.*, vol. 16, no. 4, pp. 173–175, Apr. 2006.

[22] J.-S. Paek and S. Hong, "A 29 dBm 70.7% PAE injection-locked CMOS power amplifier for PWM digitized polar transmitter," *IEEE Microw. Wireless Compon. Lett.*, vol. 20, no. 11, pp. 637–639, Nov. 2010.

[23] J. Pandey and B. P. Otis, "A sub-100 W MICS/ISM band transmitter based on injection-locking and frequency multiplication," *IEEE J. Solid-State Circuits*, vol. 46, no. 5, pp. 1049–1058, May 2011.

[24] Y.-S. Jeon, H.-S. Yang, and S. Nam, "A novel high-efficiency linear transmitter using injection-locked pulsed oscillator," *IEEE Microw. Wireless Compon. Lett.*, vol. 15, no. 4, pp. 214–216, Apr. 2005.

[25] C.-T. Chen, Y.-C. Lin, T.-S. Horng, K.-C. Peng, and C.-J. Li, "Kahn envelope elimination and restoration technique using injection-locked oscillators," in *IEEE MTT-S Int. Microw. Symp. Dig.*, Montreal, QC, Jun. 2012, pp. 1–4, Session WEPG-16.

[26] R. Adler, "A study of locking phenomena in oscillators," *Proc. IRE*, vol. 34, no. 6, pp. 351–357, Jun. 1946.

[27] L. J. Paciorek, "Injection locking of oscillators," *Proc. IEEE*, vol. 53, no. 11, pp. 1723–1727, Nov. 1965.

[28] C.-T. Chen, C.-H. Hsiao, T.-S. Horng, K.-C. Peng, and C.-J. Li, "Cognitive polar receiver using two injection-locked oscillator stages," *IEEE Trans. Microw. Theory Tech.*, vol. 59, no. 12, pp. 3484–3493, Dec. 2011.

[29] N. O. Sokal and A. D. Sokal, "Class E-a new class of high-efficiency tuned single-ended switching power amplifiers," *IEEE J. Solid-State Circuits*, vol. SSC-10, pp. 168–176, Jun. 1975.

[30] C.-T. Chen, C.-J. Li, T.-S. Horng, J.-K. Jau, and J.-Y. Li, "Design and linearization of class-E power amplifier for nonconstant envelope modulation," *IEEE Trans. Microw. Theory Tech.*, vol. 57, no. 4, pp. 957–964, Apr. 2009.

[31] Y. Li, J. Lopez, D. Y. C. Lie, K. Chen, S. Wu, T.-Y. Yang, and G.-K. Ma, "Circuits and system design of RF polar transmitters using envelope-tracking and SiGe power amplifiers for mobile WiMAX," *IEEE Trans. Circuits Syst. I, Reg. Papers*, vol. 58, no. 5, pp. 893–901, May 2011.

[32] C. D. Presti, F. Carrara, A. Scuderi, P. M. Asbeck, and G. Palmisano, "A 25 dBm digitally modulated CMOS power amplifier for WCDMA/EDGE/OFDM with adaptive digital predistortion and efficient power control," *IEEE J. Solid-State Circuits*, vol. 44, no. 7, pp. 1883–1896, Jul. 2009.

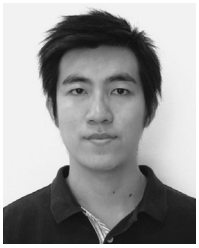

Chi-Tsan Chen (S'07–M'12) was born in Taichung, Taiwan, in 1982. He received the B.S.E.E., M.S.E.E., and Ph.D. degrees from National Sun Yat-Sen University, Kaohsiung, Taiwan, in 2005, 2007, and 2012, respectively.

He is currently a Senior Engineer with MediaTek Inc., Hsinchu, Taiwan. His research interests include RF power amplifiers, highly efficient and linear transmitter design, and low-power transceivers.

Tzyy-Sheng Horng (S'88–M'92–SM'05) was born in Taichung, Taiwan, on December 7, 1963. He received the B.S.E.E. degree from National Taiwan University, Taipei, Taiwan, in 1985, and the M.S.E.E. and Ph.D. degrees from the University of California, Los Angeles, in 1990 and 1992, respectively.

Since August 1992, he has been with the Department of Electrical Engineering, National Sun Yat-Sen University, Kaohsiung, Taiwan, where he was the Director of the Telecommunication Research and Development Center (2003–2008) and Director of the Institute of Communications Engineering (2004–2007), and where he is currently a Distinguished Professor. He has authored or coauthored over 200 technical publications published in refereed journals and conferences proceedings, mostly in IEEE publications. He holds over ten patents. His research interests include RF and microwave ICs and components, RF signal integrity for wireless system-in-package, digitally assisted RF technologies, and green radios for cognitive sensors and Doppler radars.

Dr. Horng has served on several Technical Program Committees of international conferences including the International Association of Science and Technology for Development (IASTED) International Conference on Wireless and Optical Communications, the IEEE Region 10 International Technical Conference, the IEEE International Workshop on Electrical Design of Advanced Packaging and Systems (EDAPS), the Asia–Pacific Microwave Conference, the IEEE Radio and Wireless Symposium, and the Electronic Components and Technology Conference. He has also served on the Project Review Board in the Programs of Communications Engineering and Microelectronics Engineering at the National Science Council, Taiwan. He was the recipient of the 1996 Young Scientist Award presented by the International Union of Radio Science, the 1998 Industry-Education Cooperation Award presented by the Ministry of Education, Taiwan, and the 2010 Distinguished Electrical Engineer Award presented by the Chinese Institute of Electrical Engineering, Kaohsiung Branch, Taiwan. Recently, he was awarded with the 2011 Advanced Semiconductor Engineering Inc. Chair Professorship and the 2012 Outstanding Research Award at the National Sun Yat-Sen University. He is the Founder Chair of the IEEE Microwave Theory and Techniques Society (MTT-S) Tainan Chapter and currently an associate editor of the IEEE TRANSACTIONS ON MICROWAVE THEORY AND TECHNIQUES and a member of the IEEE MTT-S Technical Committee MTT-10 and MTT-20.

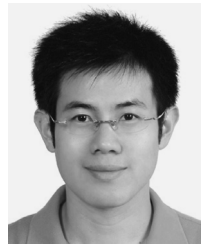

Kang-Chun Peng (S'00–M'05) was born February 18, 1976, in Taipei, Taiwan. He received the B.S.E.E., M.S.E.E., and Ph.D. degrees from the National Sun Yat-Sen University, Kaohsiung, Taiwan, in 1998, 2000 and 2005, respectively.

He is currently an Assistant Professor with the Department of Computer and Communication Engineering, National Kaohsiung First University of Science and Technology, Kaohsiung, Taiwan. His current research interests are in the area of elta–sigma modulation techniques, low-noise phase-locked loops, low-power voltage-controlled oscillators, and modulated frequency synthesizers.

Chien-Jung Li (S'07–M'10) was born in Tainan, Taiwan, on October 26, 1979. He received the B.S.E.E. and Ph.D. degrees from National Sun Yat-Sen University, Kaohsiung, Taiwan, in 2002 and 2009, respectively.

He was a Postdoctoral Fellow with the Department of Electrical Engineering, National Sun Yat-Sen University, in 2009. Following his postdoctoral position, he joined MediaTek Inc., Hsinchu, Taiwan, as a Senior Engineer, in 2010. He is currently an assistant professor with the Department of Electronic Engineering, National Taipei University of Technology, Taipei, Taiwan. His research interests include power-amplifier linearization techniques, frequency synthesizer designs, RF sensing circuits, injection-locking techniques, and LO pulling issues in direct-conversion transceivers.